Journal of Alloys and Compounds 894 (2022) 162445

Contents lists available at ScienceDirect

Journal of Alloys and Compounds

journal homepage: www.elsevier.com/locate/jalcom

Investigating the non-classical M-H_2 bonding in $OsClH_3(PPh_3)_3$

Carly C. Carter[a,1], Ryan A. Klein[b,c,1], Wei Zhou[b], Terrence J. Udovic[b,d], Craig M. Brown[b], Ting-Bin Wen[e], Thomas R. Cundari[a,*], Muhammed Yousufuddin[f,*]

[a] Department of Chemistry, University of North Texas, 1508W. Mulberry St., Denton, TX 76201, USA
[b] NIST Center for Neutron Research, National Institute of Standards and Technology, Gaithersburg, MD 20899-6102, USA
[c] Material, Chemical, and Computational Sciences Directorate, National Renewable Energy Laboratory, Golden Colorado 80401, USA
[d] Department of Materials Science and Engineering, University of Maryland, College Park, MD 20742–2115, USA
[e] College of Chemistry and Chemical Engineering, Xiamen University, Xiamen, Fujian, China
[f] Department of Natural Sciences, University of North Texas at Dallas, 7400 University Hills Blvd., Dallas, TX 75241, USA

ARTICLE INFO

Article history:
Received 19 August 2021
Received in revised form 12 October 2021
Accepted 20 October 2021
Available online 24 October 2021

Keywords:
Non-classical dihydride
Inelastic Neutron Scattering
Metal-hydride
Single-Crystal Diffraction
Hydrogen Storage Materials
Osmium

ABSTRACT

Dihydrogen ligation to metal centers results in a wide range of metal-hydrogen interactions. Compounds containing non-classical dihydrogen ligands in which the H–H contacts are significantly longer than the 0.74 Å distance found in solid H_2 are classified as Kubas-like compounds, stretched dihydrogen ligands, or compressed dihydrides, depending on the H–H contact length. Compounds containing stretched dihydrogen and compressed dihydride ligands are somewhat rare. Developing a more complete understanding of the metal-hydrogen and hydrogen-hydrogen interactions in these species may provide insights into the mechanisms for the oxidative addition reaction and hydrogen storage. Here, we use diffraction and inelastic neutron scattering (INS) measurements, paired with both molecular and solid-state density functional theory (DFT), to fully characterize the nature of the metal-hydrogen and hydrogen-hydrogen interactions in a previously reported compound, $OsClH_3(PPh_3)_3$. In that report, the H–H distance was measured as 1.48(2) Å by single-crystal neutron diffraction and was described as a "stretched" dihydrogen. The INS-generated phonon density of states is well described by the DFT calculations, including those normal modes dominated by the vibrational motions of the three Os-ligated hydrogen atoms. The resulting calculated electron charge density landscape indicates that there is no remnant bonding character between the Os-ligated hydrogen atoms in the compound. Based on these findings, we update the understanding of the metal-hydrogen bonding in this complex and reclassify it as a compressed dihydride. As such, $OsClH_3(PPh_3)_3$ represents a rare example of a non-classical compressed dihydride species.

1. Introduction

The non-classical dihydrogen ligand has garnered considerable interest since its discovery by Kubas and coworkers in 1984 [1–3]. The H–H distances, d_{HH}, in non-classical ligands range between ≈ 0.8–1.6 Å [4]. Within this range, the H_2 moiety exists as three distinct classes: Kubas-like H_2 ligands (d_{hh} range of ≈ 0.8–1.0 Å), stretched dihydrogen ligands (≈ 1.0–1.25 Å), and compressed dihydrides (≈ 1.25–1.6 Å, Fig. 1). Values of d_{HH} greater than 1.6 Å arise in classical terminal polyhydridic species [4,5]. A closer inspection of the H–H interaction in M–H_2 systems (where M is a metal center) shows that as metal-ligated d_{HH} elongates, the d_{MH} distances begin to shorten and the H-M-H angles begin to widen. Each interaction depicted in Scheme 1—Kubas-like dihydrogen (**I**), stretched dihydrogen (**II**), compressed dihydride (**III**), and classical dihydride (**IV**)—can be seen as a snapshot along the reaction coordinate for the oxidative addition of H_2 to a metal center. Further studies into the M–H_2 interaction are key to better understanding oxidative addition, which is involved in many catalytic processes [6,7]. Moreover, dihydrogen ligation to coordinatively unsaturated metal centers in porous adsorbates is one possible synthetic strategy for increasing the storage capacities at operationally relevant conditions in candidate hydrogen storage materials [8–12]. A better understanding of the metal-ligand interactions in metal-dihydrogen complexes may lead to better hydrogen storage materials, which require an optimal interaction enthalpy to enable reversible room temperature storage [13].

* Corresponding authors.
E-mail addresses: t@unt.edu (T.R. Cundari), myousuf@untdallas.edu (M. Yousufuddin).
[1] C.C.C. and R.A.K. contributed equally to this work

https://doi.org/10.1016/j.jallcom.2021.162445
0925-8388/

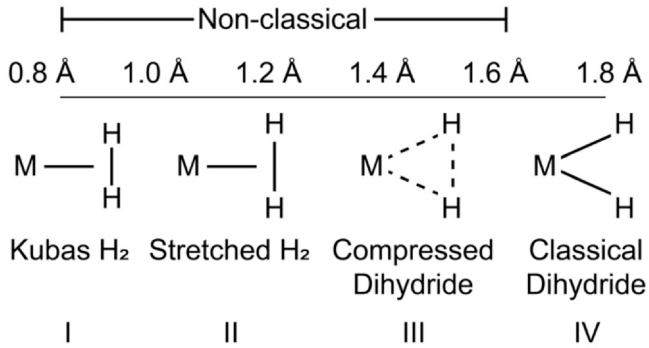

Scheme 1. The approximate ranges of d_{HH} distances in the different classes of M-H_2 compounds are shown for non-classical (I, II, III) and classical species (IV).

Compounds displaying intermediate d_{HH} distances between 1.0 Å and 1.6 Å are somewhat rare. These compounds bridge the gap between non-classical Kubas-like dihydrogen and the classical dihydride ligands [4]. At some d_{HH} distance between the two end states **I** and **IV** in Scheme 1, the H–H bond is broken [14]. Deeper insight into the electronic and steric influences of the other ligands in the metal center's coordination sphere on the M–H and H–H bonding in these intermediate species will help to refine the synthetic criteria used in the design of new candidate hydrogen storage materials [15]. And even in the cases where the Kubas-like complexes contain metals that may be too expensive or too heavy for suitable hydrogen storage materials, useful structural information can still be gleaned.

One of the early molecules displaying an intermediate d_{HH} contact length was $OsClH_3(PPh_3)_3$ (PPh_3 = triphenylphosphine) [16], The neutron-derived crystal structure revealed H–H contact distances of 1.48(2) Å and 1.67(2) Å, suggesting the presence of a non-classical "stretched" H_2 ligand adjacent to a classical terminal hydride (Fig. 1). Based on the crystal structure, there was hypothesized to be some remnant bonding character between H2 and H3, even though the observed d_{HH} contact length is nearly double that of H_2 in the solid state [17]. At the same time, the d_{OsH} distances of 1.60(2) Å (H2), 1.61(2) Å (H3), and 1.62(2) Å (H1) are on the cusp of the expected distance for classical terminal hydride ligands [18,19], potentially suggesting a lack of any remnant bonding interaction between the hydrogen atoms in the complex. The crystal structure alone is therefore insufficient for providing a detailed understanding of the nature of the M–H and H–H bonding interactions present in $OsClH_3(PPh_3)_3$. Spectroscopic studies coupled with first principles calculations are required to develop a better understanding of these bonding interactions. A previous NMR study found a relaxation time that hinted at a non-classical interaction of the hydrogen atoms in this compound (T_1 = 26 ms at −40 °C and 300 MHz in C_6D_6) [20]. However, the hydride signals coalesced at − 40 °C and the T_1 value could have been affected by the dissociation of ligands present in the compound. Unfortunately, a minimum T_1 value could not be determined because of low solubility of the complex at low temperatures which hindered the complete characterization of the nature of the H–H and M–H bonding interactions in this complex by NMR.

Herein, we revisit $OsClH_3(PPh_3)_3$ (**1**) and study the M–H and H–H bonding interactions using single-crystal X-ray diffraction (SCXRD) measurements, inelastic neutron scattering (INS) measurements, and density functional theory (DFT) calculations [21]. The interpretation of the INS data is supported by DFT phonon calculations. Animations of the calculated phonon modes greatly facilitate assignment of the spectral features. In addition, optimized geometry calculations for $OsFH_3(PPh_3)_3$, $OsBrH_3(PPh_3)_3$, $OsIH_3(PPh_3)_3$, and $OsH_4(PPh_3)_3$ provide insight into the effect of the *trans* ligand on the nature of the M–H and H–H interactions.

2. Experimental section

2.1. Synthesis of 1

The title complex was prepared as described previously [20]. 20 mL of benzene were added to 0.095 mmol of $OsCl_2(PPh_3)$ and stirred until dissolved. 20 μL of NEt_3 were added and the entire solution was frozen by placing the reaction flask in liquid nitrogen. After freezing, the reaction flask was evacuated and filled with 600 mmHg of H_2. The flask was then allowed to warm to room temperature and stirred for 1.5 h, yielding a pale green solution. Crystals were grown by layering a minimum amount of n-hexane over a dichloromethane solution of the compound under an atmosphere of dihydrogen gas.

2.2. Single-crystal X-ray diffraction

SCXRD data for **1** were collected using a Bruker Smart APEX diffractometer[2] with Mo-K_α radiation (λ = 0.71073 Å). The cell parameters were obtained from the least squares refinement of the spots (from 60 collected frames) using SMART [22]. The data collection was performed using SMART and data processing was performed using the SAINT program [22]. Initial atomic positions were located using direct methods. The structure was corrected for absorption effects using SADABS [23] and refined by least squares methods using SHELXL2018 [24]. Calculated hydrogen atom positions for the phenyl rings were input and refined in a riding manner along with their corresponding carbon atoms. Hydrogen atoms ligated to osmium atoms were not located. The X-ray crystallographic details are summarized in Table S1 in the Supporting Information.

2.3. Inelastic neutron scattering

The neutron vibrational spectrum for **1** between 33 meV (266 cm^{-1}) and 200 meV (1613 cm^{-1}) in neutron energy loss was measured at the National Institute of Standards and Technology Center for Neutron Research (NCNR) with the BT-4 Filter Analyzer Neutron Spectrometer. The experiment used horizontal 20′ collimations before and after the Cu(220) monochromator [25]. Because of the air-sensitive nature of the compound, ≈ 1 g of the sample was loaded while under inert atmosphere into a hermetically sealed Al sample holder. The sample was cooled to 4 K and data were collected for 1 day. Additional INS spectra at lower energy transfer values were measured for **1** using the Disk Chopper Spectrometer (DCS) [26] at the NCNR. Spectra at 4 K were collected using incident neutron wavelengths of both 6 Å and 9 Å on the same sealed sample. The spectral range probed in these measurements was between a neutron energy gain of ≈ 18 meV (≈145 cm^{-1}) and a neutron energy loss of 2 meV (≈16 cm^{-1}).

2.4. Phonon mode calculation and INS simulation

First-principles DFT calculations for **1** were performed using the Quantum ESPRESSO package [27]. For these calculations, we used Vanderbilt-type ultrasoft pseudopotentials with Perdew–Burke–Ernzerhof exchange correlations. A cut-off energy of 544 eV and a 1 × 2 × 1 *k*-point mesh was used and found to be sufficient for the total energies to converge within 0.01 meV $atom^{-1}$. The crystal structure of **1** was fully optimized with respect to the atomic coordinates prior to using the finite differences method to calculate the

[2] Certain commercial equipment, instruments, or materials are identified in this document. Such identification does not imply recommendation or endorsement by the National Institute of Standards and Technology, nor does it imply that the products identified are necessarily the best available for the purpose.

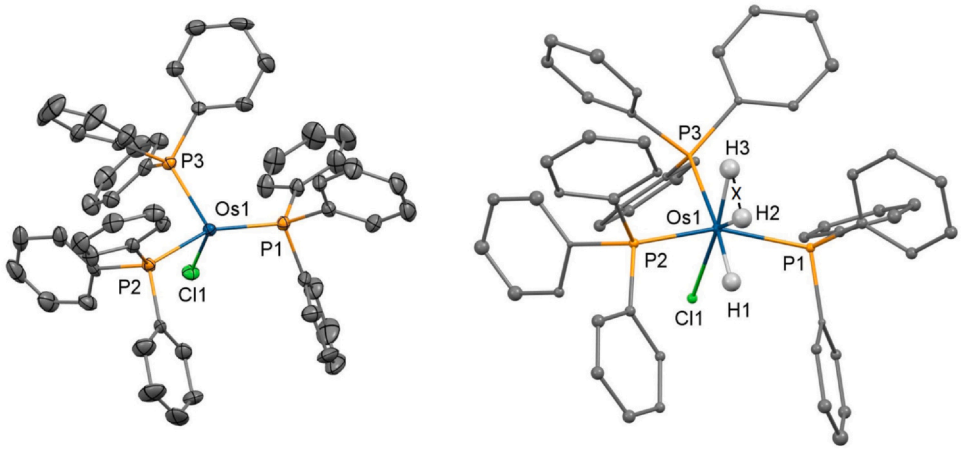

Fig. 1. Full molecular core of 1. The X-ray-derived structure is depicted on the left and the neutron-derived structure, adapted from reference 16, is depicted on the right. Ellipsoids in the X-ray structure are drawn at 30% probability. Atoms in the neutron structure were refined isotropically. Hydrogen atoms associated with the PPh_3 ligands are omitted for clarity. Blue, green, orange, gray, and white spheres represent Os, Cl, P, C, and H atoms, respectively. "X" in the neutron structure between H2 and H3 designates the center of the H-H distance. The d_{HH} distance is 1.48(2) Å as measured by single-crystal neutron diffraction.

phonons. INS spectra were further simulated within the incoherent approximation, with the neutron scattering cross sections of the different elements appropriately weighted and the instrumental resolution taken into account.

2.5. Geometry optimization calculations

The crystal unit cell of **1** is large (containing 428 atoms). Therefore, we used the more efficient hybrid quantum mechanics/molecular mechanics (QM/MM) approach to optimize and determine the geometry and frequencies of several osmium compounds [$OsFH_3(PPh_3)_3$, $OsClH_3(PPh_3)_3$, $OsBrH_3(PPh_3)_3$, and $OsIH_3(PPh_3)_3$] with ONIOM (ωB97XD /GenECO:UFF) methods. The basis set 6–311 + +G(d,p) was used for the C, H, P, Cl, F, and Br atoms and basis set CEP-31 G for the Os atoms. QM was used on the osmium atom and the atoms bonded to it while the UFF was used on the peripheral groups attached to the phosphines. These molecular DFT simulations were done at standard temperature (298.15 K) and pressure (1 atm) in the gas phase on single molecules using the software package Gaussian 16 [28].

3. Results and discussion

3.1. Crystal structure of 1

Fig. 1 shows the plot of the title compound. The coordination geometry for the metal center resembles a severely distorted octahedron or pentagonal bipyramid. The Os–P distances vary between 2.327(11) Å and 2.439(10) Å in the neutron study and between 2.3423(19) Å and 2.459(2) Å in the X-ray study. The P1-Os-P2 angle for the *trans* P atoms is 155.2(4)° in the neutron study and 156.12(9)° in the X-ray study. The previous neutron study shows that the terminal hydride (H1) is *trans* to a P atom and the P3-Os-H1 angle is somewhat linear at 172.5(6)°. The Cl-Os-X (where X is the center between the two H atoms) is also fairly linear at 171.4(3)°. The average P-Os-P angles for the *cis* P atoms are 102.3(4)° from the neutron structure and 101.80(8)° from the X-ray study. The chloride ligand-to-metal distance agrees well at 2.467(6) Å and 2.463(2) Å from the neutron and X-ray studies, respectively.

From the previous neutron study [16], all three H atoms and the chloride ligand lie approximately in the same plane, while the P1-P2-P3-H1 atoms lie in an intersecting plane. However, P1-P2-Cl1-X should all be in the same plane in a perfect octahedron, but this plane is severely distorted. The source of the distortion appears to be the bulky phosphine ligands and their mutual repulsion (the average cone angle for the phosphine ligands from the X-ray study was estimated to be ~145°). A list of selected bond distances from the X-ray and the previous neutron study are compared in Table S2 in the Supporting Information.

3.2. Inelastic neutron scattering

The neutron-fast-background-corrected INS spectrum for **1** is shown in red in Fig. 2. The 1 + 2-phonon spectrum calculated for **1** (using plane-wave periodic DFT method) is shown below the experimental data as the dark gray curve (the light gray curve is the 1-phonon spectrum). Visual inspection shows good agreement between the calculated and observed spectra. From these calculations, the modes involving the three H atoms ligated to the Os center were identified and isolated. In Fig. 2, the blue curve (denoted as '3 H only' in the legend) corresponds to the calculated 1-phonon spectrum for the structure in which the scattering cross section was artificially set to zero for all atoms except the three metal-ligated H atoms. To corroborate this approach, the 1-phonon spectrum for the selectively deuterated $OsClD_3(PPh_3)_3$ was calculated and subtracted from the 1-phonon spectrum for **1** (Fig. 2, maroon curve). Since the neutron scattering cross section for D is much smaller than for H [29], such a subtraction should yield a similar spectrum to the blue curve, i.e., one that largely removes the scattering contributions from all compound atoms except the three Os-ligated H atoms. Again, visual inspection shows good agreement between the difference curve and the 1-phonon spectrum calculated for the Os-ligated H atoms only.

Animations of the calculated phonon modes reveal the precise nature of each of the observed features in the spectra. We visualized these animations, with the.ascii file included with the Supporting Information, using the v_sim software package [30]. Upon investigating the animations, we find that the strong modes in the spectrum calculated for Os-ligated H atoms at ≈ 58.99 meV and ≈ 63.73 meV are rocking/twisting modes of the OsH_3 core, the mode at ≈ 89.51 meV is a wagging/twisting mode, and the features at ≈ 104.10 meV and ≈ 116.43 meV correspond to bending/rocking modes. For the two higher-energy modes, the $\delta(OsH_2)$ bending motion occurs as the H2 and H3 atoms move along the H–H coordinate. This motion is accompanied by in-phase OsH_3 rocking. The complementary mode with $\delta(OsH_2)$ bending for H2 and H3 with out-of-phase OsH_3 rocking occurs at significantly lower energy, ≈ 53.36 meV. However, this motion is accompanied by movement of

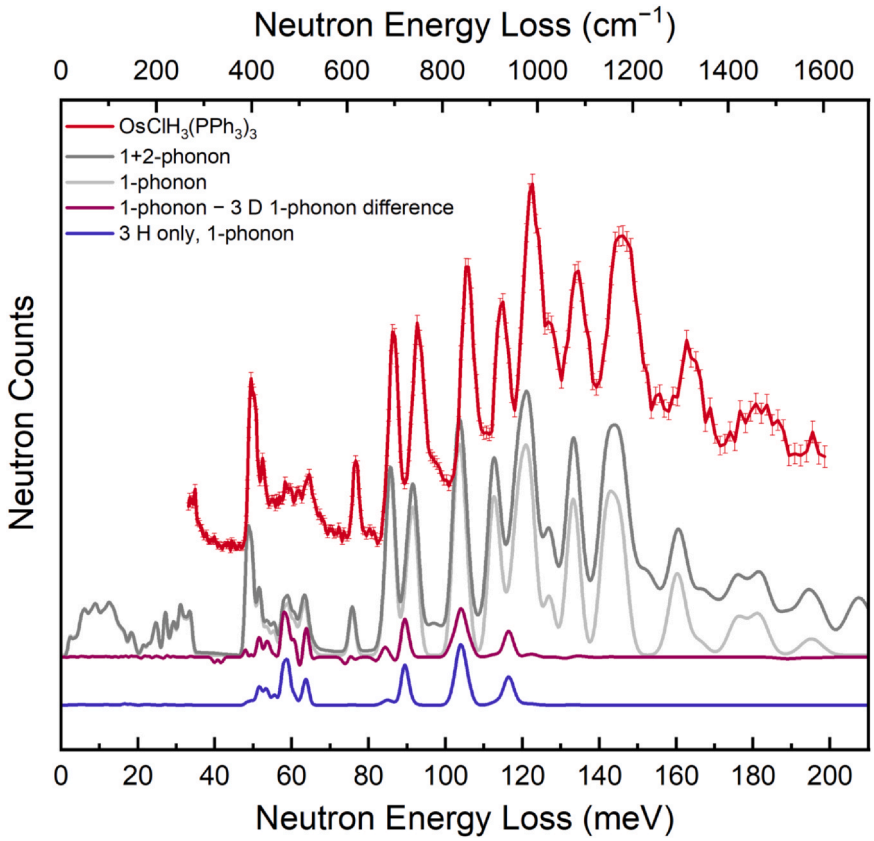

Fig. 2. The measured (red) and calculated (other colors) INS spectra for $OsClD_3(PPh_3)_3$between 0 and 210 meV. The respective dark gray and light gray curves represent the calculated 1 + 2-phonon and 1-phonon spectra for **1**. The blue curve shows the calculated modes for just the three H atoms ligated to the metal. The maroon curve is the difference curve for the calculated 1-phonon spectrum for **1** minus the calculated 1-phonon spectrum for $OsClD_3(PPh_3)_3$. Error bars correspond to ± 1σ.

the relatively heavy phosphines which lowers the energy of the mode. We note that, although some of the phonon spectral features associated with the three metal-ligated H atoms involve mostly H atom displacements, a comparison with the total compound spectrum indicates the marked presence of other overlapping normal modes at similar energies that involve a significant motional mixing of these three H atoms with the other substituent atoms. The presence of such resonant mixing has obscured assignment of metal-dihydrogen modes in previous reports [31].

The calculations for modes present at higher energies outside our measurement window (Fig. S1 in the Supporting Information) indicate an intense band at ≈ 266.44 meV correlating to a ν_{sym}(Os–H_2) mode for H1 and H3 mixed with a ν(Os–H2) mode. Then, at slightly higher energies, the calculations indicate a shoulder to this feature which corresponds to a ν_{sym}(Os–H_2) mode for H1 and H3 mixed with a ν(Os–H2) motion at ≈ 276.72 meV. These calculated modes suggest a lack of any remnant bonding character between the H2 and H3 atoms.

The observed hydrogen-specific modes in the measured spectral window share similarities with both classical and non-classical molecular polyhydride compounds. The observed ν_{sym}(OsH) and δ(OsH_2) modes fall within the range expected for classical terminal hydride ν_{sym}(OsH) stretching (≈ 245–270 meV) and bending (≈ 80–110 meV) modes [32,33]. Yet the lower-energy modes are distinct from the terminal hydride species (i.e. those between 45 and 60 meV, which correspond to rocking, bending, twisting, and wagging modes for the metal-ligated H atoms in **1**). Instead, they are similar to the features expected for Kubas complex-like η^2-H_2 ligands, which display five modes upon complexing to a metal center (symmetric stretching, asymmetric stretching, in-plane bending, out-of-plane bending, and torsional modes). For η^2-H_2 ligands, ν_{sym}(HH) ranges from ≈ 260–400 meV while ν_{as}(HH) ranges between ≈ 165 meV and 200 meV [34–36]. The ν_{sym}(MH_2) modes for Kubas-like dihydrogen ligands can be as low as ≈ 84 meV with δ(MH_2) modes as low in energy as 50 meV, for example, in [Ru(C_5H_5)($Ph_2PCH_2PPh_2$)(η^2–H_2)][BF_4] [37]. Specific examples in Os polyhydrides are somewhat rare because, while many Os polyhydridic compounds have been isolated [38–40], only a handful have been interrogated using vibrational spectroscopy coupled with first-principles calculations. One example is Cp*OsH_4(L)$_3$ (L = PPh_3, $AsPh_3$, and PCy_3, PCy_3 = tricyclohexylphosphine), where the compounds were characterized crystallographically using single-crystal neutron diffraction measurements and via vibrational spectroscopy techniques [41]. Assessment of the crystal structures shows that the H_2 ligand is found to be of Kubas complex-like nature for L = PPh_3 and $AsPh_3$ but of compressed dihydride character for L = PCy_3. IR measurements reveal ν_{sym}(OsH) modes at ≈ 260 meV for all three compounds, despite different d_{HH} distances of 1.01 Å, 1.08 Å, and 1.31 Å, respectively [42]. INS measurements of the triphenylphosphine compound indicate the τ(HH) torsional mode occurs at ≈ 41.5 meV, δ(OsH_2) at ≈ 48.4 meV, and rocking/wagging at ≈ 60.8 meV [43]. These modes are similar to the features observed in the INS spectra reported here, despite the differences in d_{HH} of 1.01 Å for Cp*$OsH_4(PPh_3)_3$ compared to the d_{HH} of 1.48(2) Å for **1**. Given these similarities, the additional modes at moderate energy transfer values observed herein support the non-classical nature of the close H-H contact for **1**.

The INS spectra for **1** measured at lower energy transfer values (−18 to 2 meV neutron energy loss) with DCS using both 6 Å and 9 Å incident neutron wavelengths indicated no extra scattering features except the elastic scattering. In both cases, the entire spectrum can be well fit using a delta function convoluted with the instrumental

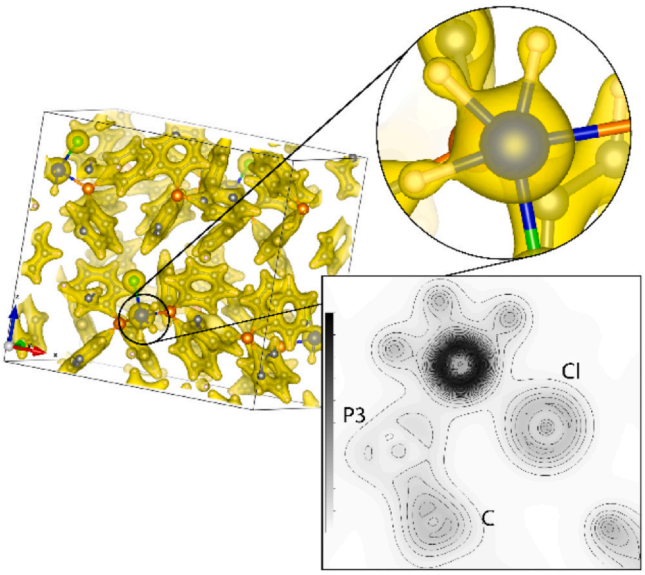

Fig. 3. The electron charge density map for **1** for one unit cell is shown at an isosurface level of 0.14 e bohr^{-3}. The enlarged insets illustrate the calculated charge density locally around the OsH_3 core. The topography style map contains contours at every 5% of saturation between 0% and 100% e bohr^{-3} saturation on a section of the slice of the cell along the (470) crystallographic plane. Blue, white, orange, and gray, and green spheres represent Os, H, P, C, and Cl atoms, respectively. Note that the OsH_3 core in the enlarged, rounded inset is reoriented to better display the moiety and does not directly correspond to the location indicated in the depicted unit cell.

resolution function. In contrast, molecular systems containing an η^2–H_2 ligand display broad features in the INS data near the elastic line which arise from the rotational excitations of the H_2 molecule about the M–H_2 axis [44]. The lack of any features between ≈ −18 meV and 2 meV here suggests that the H2 and H3 atoms ligated to the Os center in **1** do not rotate about an M–H_2 axis and are best described as terminal compressed dihydrides. A representative INS Spectrum collected on the DCS instrument is included as Fig. S2 (and Fig. S3) in the Supporting Information.

Lastly, the DFT-calculated electron charge density was plotted for **1** (Fig. 3). A section of the crystallographic (470) plane is displayed in Fig. 3, as a contour plot, with contours at 5% e bohr^{-3} intervals. This plot illustrates the lack of electron density between the Os-ligated H atoms, further suggesting that these H atoms are non-classical compressed terminal hydride ligands.

3.3. Computational QM/MM results

Optimized geometries were computed for **1** (Fig. 4, top middle). The calculated H–H distance of 1.573 Å is somewhat longer than the measured distance of 1.48(2) Å, and just at the cusp of a terminal hydride ligand. However, the calculated and measured Os–H distances agree reasonably well. The calculated Os–H average was measured as 1.59(1) Å while the measured average Os–H distance from neutron diffraction is 1.608(15) Å. The computed geometries involving H atoms are also comparable to measured values. The H2-Os-H3 angle was measured as 55.1(8)° compared to the computed angle of 58.97°. Table S2 in the Supporting Information compares selected bond distances from optimized geometries to the neutron- and X-ray-derived structures.

To further investigate the effects of the *trans* ligand on the M–H and H–H interactions, optimized geometries were calculated for $OsFH_3(PPh_3)_3$, $OsBrH_3(PPh_3)_3$, and $OsIH_3(PPh_3)_3$ (Fig. 4). The H–H distance in the non-classical dihydrogen ligand seems to vary depending on the halide *trans* to the dihydrogen ligand. For

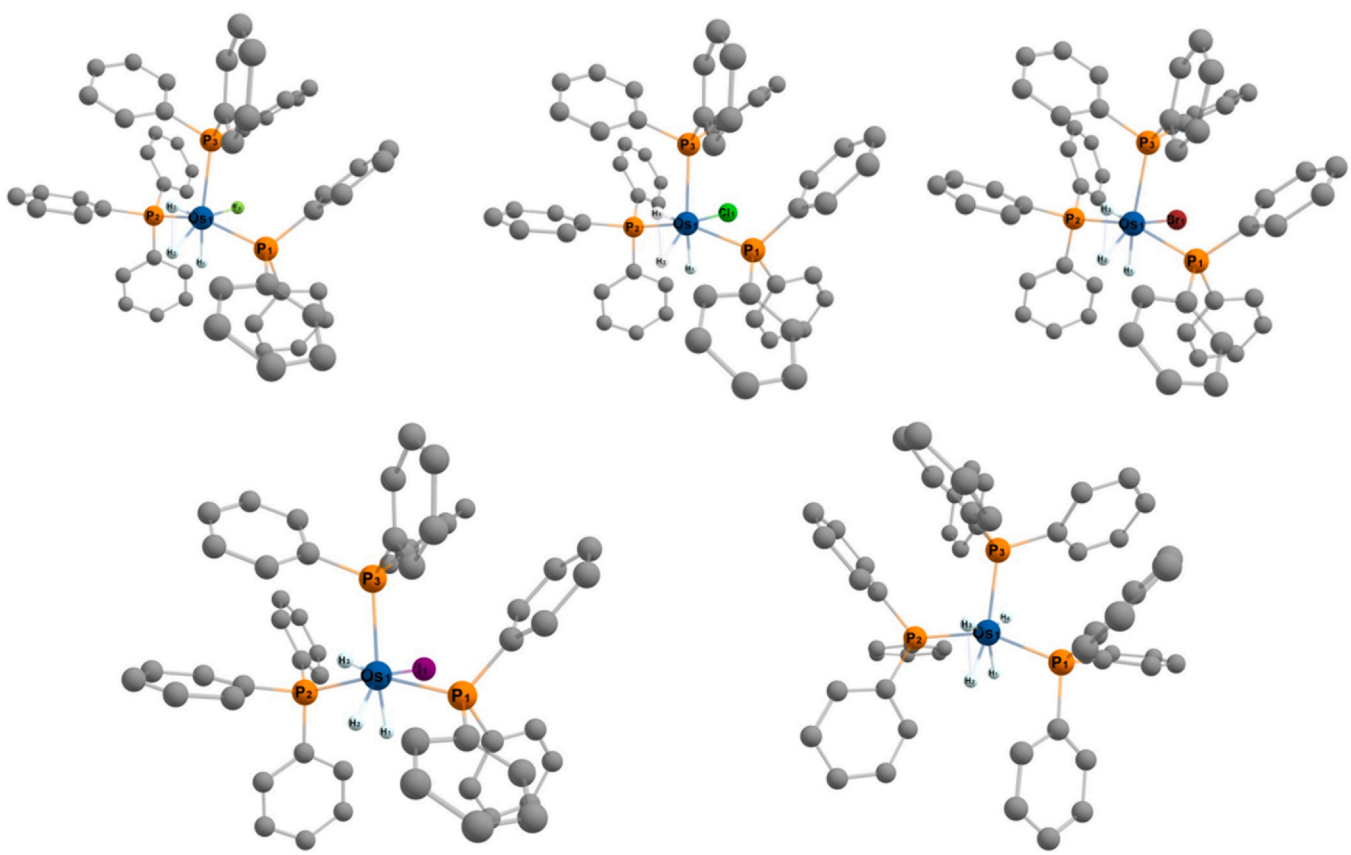

Fig. 4. DFT optimized structures of $OsFH_3(PPh_3)_3$ (top left), $OsClH_3(PPh_3)_3$ (top middle), $OsBrH_3(PPh_3)_3$ (top right), $OsIH_3(PPh_3)_3$ (bottom left), and $OsH_4(PPh_3)_3$ (bottom right). H atoms attached to phenyl groups omitted for clarity.

$OsFH_3(PPh_3)_3$, $OsClH_3(PPh_3)_3$, $OsBrH_3(PPh_3)_3$, and $OsIH_3(PPh_3)_3$ the H–H distances are 1.510 Å, 1.573 Å, 1.602 Å, and 1.636 Å, respectively. This demonstrates a trend that, as electronegativity of the *trans* ligand increases, H–H distances decrease, through the threshold definition d_{HH} length for a classical to a non-classical dihydride (1.6 Å).

We also see the Os–L (where L is a halide) distance increase as the halogen radius increases. Interestingly, the X-Os-L angle (where X is the midway point between H2 and H3) stays reasonably linear for all three structures. Table S3 in the Supporting Information compares selected bond distances and angles for optimized structures of $OsFH_3(PPh_3)_3$, $OsClH_3(PPh_3)_3$, $OsBrH_3(PPh_3)_3$, and $OsIH_3(PPh_3)_3$. As a final comparison, we calculated the optimized geometry of the tetrahydride $OsH_4(PPh_3)_3$, which shows a classical polyhydride structure (Fig. 4, bottom right). This structure contains no halide *trans* to the centroid of the H atoms and the H–H distance increases to 1.819 Å, further confirming the role of the *trans* ligand in stabilizing a non-classical compressed dihydride species. Table S3 in the Supporting Information includes selected $OsH_4(PPh_3)_3$ bond distances and angles.

It should be noted that the neutron structure of the analogous tetrahydride $OsH_4(PPhMe_2)_3$ was previously reported [18]. Because $OsH_4(PPh_3)_3$ is similar to $OsH_4(PPhMe_2)_3$, we were interested in comparing the core of the optimized structure for $OsH_4(PPh_3)_3$ to the core of the neutron structure of $OsH_4(PPhMe_2)_3$, as the main difference between these two structures is the phosphine ligand. A comparison of distances and angles from both structures shows reasonable agreement. Considering just Os–H1, Os–H2, and Os–H3 and the corresponding hydrides of the neutron structure, the average computed Os–H distance is 1.643(36) Å compared to the measured average Os–H distance from neutron diffraction of 1.658(20) Å. The average H-Os-H angle for both structures is also quite similar, at 90.55(39)° for the optimized structure versus 91.92(39) for the neutron structure. And, although $OsH_4(PPhMe_2)_3$ contains smaller phosphine ligands, the average P-Os-P angles for $OsH_4(PPh_3)_3$ were computed as 119.73(30)° compared to the measured average of 120.00(39)° for the neutron structure of $OsH_4(PPhMe_2)_3$. The agreement between the calculated structure for $OsH_4(PPh_3)_3$ with the neutron-derived structure for $OsH_4(PPh_2Me)_3$ validates the choice of functionals used in the geometry optimization calculations.

4. Conclusion

We have revisited the $OsClH_3(PPh_3)_3$ complex, **1**, previously described in the literature as a stretched dihydrogen complex. Herein we probe the M–H and H–H bonding interactions using INS measurements coupled with first-principles calculations, and by comparing the measured crystal structure to calculated optimized geometry structures. Based on the analysis of the INS spectra reported here, we conclude that there is no remnant bonding character between the close H atoms in **1** and we reassign the ligands as non-classical compressed dihydride ligands (H2 and H3) adjacent to a classical terminal hydride (H1). Interestingly, calculated optimized geometries suggest that d_{HH} decreases with increasing electronegativity of the *trans* halide. The ability to tune the nature of the M (H_2) interaction via modulation of the supporting ligands in the present $OsXH_3(PR_3)_3$ and related complexes can be beneficial for rationally increasing the volumetric hydrogen storage capacity in metal hydride materials and in porous adsorbate materials decorated with coordinatively unsaturated metal centers. Moreover, the integration of synthetic, spectroscopic and computational tools to study such $M(H_2)$ entities provides a protocol for assessing how such structural changes can impact properties relevant to these important applications.

CRediT authorship contribution statement

Carly C. Carter: Investigation, Formal Analysis. **Ryan A. Klein:** Writing – original draft, Visualization. **Wei Zhou:** Investigation, Formal Analysis. **Terrence J. Udovic:** Investigation, Writing – review & editing, **Craig M. Brown:** Investigation, Writing – review & editing. **Ting-Bin Wen:** Investigation. **Thomas R. Cundari:** Supervision, Writing – review & editing, Funding Acquisition. **Muhammed Yousufuddin:** Conceptualization, Investigation, Writing – original draft.

Declaration of Competing Interest

The authors declare that they have no known competing financial interests or personal relationships that could have appeared to influence the work reported in this paper.

Acknowledgements

M.Y. thanks the University of North Texas at Dallas for partial support. C.C.C. and T.R.C. acknowledge the National Science Foundation for partial support through grants CHE-1464943 and CHE-1531468 (for computing equipment). R.A.K. acknowledges research support from the Hydrogen Materials - Advanced Research Consortium (HyMARC), established as part of the Energy Materials Network under the U.S. Department of Energy, Office of Energy Efficiency and Renewable Energy, Hydrogen and Fuel Cell Technologies office, under contract number DE-AC36-8GO28308 to the National Renewable Energy Laboratory (NREL). This work utilized neutron scattering facilities supported in part by the National Science Foundation under Agreement No. DMR-0454672. Phonon calculations were performed on the NIST Enki HPC cluster. The authors are grateful to Prof. Guochen Jia for his assistance with the manuscript preparation. The views expressed in the article do not necessarily represent the views of the DOE or the U.S. Government. The U.S. Government retains and the publisher, by accepting the article for publication, acknowledges that the U.S. Government retains a nonexclusive, paid-up, irrevocable, worldwide license to publish or reproduce the published form of this work, or allow others to do so, for U.S. Government purposes.

Appendix A. Supplementary material

Supplementary data associated with this article can be found in the online version at doi:10.1016/j.jallcom.2021.162445.

References

[1] G.J. Kubas, R.R. Ryan, B.I. Swanson, P.J. Vergamini, H.J. Wasserman, Evidence for a side-on bonded H2 ligand, J. Am. Chem. Soc. 106 (1984) 451–452.
[2] P.G. Jessop, R.H. Morris, Reactions of transition metal dihydrogen complexes, Coord. Chem. Rev. 121 (1992) 155–284.
[3] D. Heinekey, W.J. Oldham, Coordination chemistry of dihydrogen, Chem. Rev. 93 (1993) 913–926.
[4] G.G. Hlatky, R.H. Crabtree, Transition-metal polyhydride complexes, Coord. Chem. Rev. 65 (1985) 1–48.
[5] G.O. Spessard, G.L. Miessler, Organometallic Chemistry, Oxford University Press, 2009.
[6] R.H. Crabtree, The Organometallic Chemistry of the Transition Metals, 6th ed., John Wiley & Sons, 2009.
[7] R.H. Crabtree, Dihydrogen complexation, Chem. Rev. 116 (2016) 8750–8769.
[8] K.M. Thomas, Hydrogen adsorption and storage on porous materials, Catal. Today 120 (2007) 389–398.
[9] M. Hirscher, V.A. Yartys, M. Baricco, J.B. von Colbe, D. Blanchard, R.C. Bowman Jr., D.P. Broom, C.E. Buckley, F. Chang, P. Chen, et al., Materials for hydrogen-based energy storage–past, recent progress and future outlook, J. Alloy. Compd. 827 (2020) 153548.

[10] M.T. Kapelewski, T. Runčevski, J.D. Tarver, H.Z.H. Jiang, K.E. Hurst, P.A. Parilla, A. Ayala, T. Gennett, T.S.A. FitzGerald, C.M. Brown, J.R. Long, Record high hydrogen storage capacity in the metal–organic framework Ni2(m-dobdc) at near-ambient temperatures, Chem. Mater. 30 (2018) 8179–8189.
[11] D.E. Jaramillo, H.Z.H. Jiang, H.A. Evans, R. Chakraborty, H. Furukawa, C.M. Brown, M. Head-Gordon, J.R. Long, Ambienttemperature hydrogen storage via vanadium (II)-dihydrogen complexation in a metal–organic framework, J. Am. Chem. Soc. 143 (2021) 6248–6256.
[12] R.A. Klein, H.A. Evans, B.A. Trump, T.J. Udovic, C.M. Brown, Neutron scattering studies of materials for hydrogen storage, reference module in chemistry, Molecular Sciences and Chemical Engineering, Elsevier, 2021.
[13] S.K. Bhatia, A.L. Myers, Optimum conditions for adsorptive storage, Langmuir 22 (2006) 1688–1700.
[14] D.M. Heinekey, A. Lledós, J.M. Lluch, Elongated dihydrogen complexes: what remains of the H–H bond? Chem. Soc. Rev. 33 (2004) 175–182.
[15] T. Runčevski, M.T. Kapelewski, R.M. Torres-Gavosto, J.D. Tarver, C.M. Brown, J.R. Long, Adsorption of two gas molecules at a single metal site in a metal–organic framework, Chem. Comm. 52 (2006) 8251–8254.
[16] M. Yousufuddin, T.B. Wen, S.A. Mason, G.J. McIntyre, G. Jia, R.A. Bau, Neutron diffraction study of [OsClH3(PPh3)3]: a complex containing a highly ——stretched‖ dihydrogen ligand, Angew. Chem. Int. Ed. 44 (2005) 7227–7230.
[17] J.V. Kranendonk, H. Gush, The crystal structure of solid hydrogen, Phys. Lett. (1962) 1.
[18] D.W. Hart, R. Bau, T.F. Koetzle, Neutron and X-ray diffraction studies on tris(dimethylphenylphosphine) osmium tetrahydride, J. Am. Chem. Soc. 99 (1977) 7557–7564.
[19] J.A. Howard, O. Johnson, T.F. Koetzle, J.L. Spencer, Crystal and Molecular Structure of bis(diisopropylphenylphosphine) hexahydridoosmium,[OsH6(PC12H19)2]: Single-Crystal Neutron Diffraction Study at 20 K, Inorg. Chem. 26 (1987) 2930–2933.
[20] G. Ferrando, K.G. Caulton, Dehydrohalogenation as a Source of OsHnCl(PPh3)3 (n = 1, 3), Inorg. Chem. 38 (1999) 4168–4170.
[21] S.W. Lovesey, The Theory of Neutron Scattering from Condensed, Matter, Oxford University Press, 1986.
[22] Bruker-AXS, 2000, Madison, WI, USA.
[23] Bruker-AXS, 2006, Madison, WI, USA.
[24] G.M. Sheldrick, Crystal structure refinement with SHELXL, Acta Cryst. C. 71 (2015) 3–8.
[25] T.J. Udovic, C.M. Brown, J.B. Leão, P.C. Brand, R.D. Jiggetts, R. Zeitoun, T.A. Pierce, I. Peral, J.R.D. Copley, Q. Huang, D.A. Neumann, R.J. Fields, The design of a bismuth-based auxiliary filter for the removal of spurious background scattering associated with filter-analyzer neutron spectrometers, Nucl. Instr. Meth. A 588 (2008) 406–413.
[26] J.R.D. Copley, J.C. Cook, The disk chopper spectrometer at NIST: a new instrument for quasielastic neutron scattering studies, Chem. Phys. 292 (2003) 477–485.
[27] P. Giannozzi, O. Andreussi, T. Brumme, O. Bunau, M.B. Nardelli, M. Calandra, R. Car, C. Cavazzoni, D. Ceresoli, M. Cococcioni, et al., Advanced capabilities for materials modelling with quantum ESPRESSO, J. Phys.: Condens. Matter 29 (2017) 465901.
[28] Gaussian 16, Revison A.03, M.J. Frisch et. al.Gaussian, Inc. Wallingford CT, 2016.
[29] V.F. Sears, Neutron scattering lengths and cross sections, Neutron N. 3 (1992) 26–37.
[30] L. Billard, D. Caliste, D. Olivier, A. Lherbier, B. Jérémy, P. Simon, T. Jourdan, T. Ratao, V_sim, http://www.memlab.fr/en/Pages/L_SIM/Softwares/V_Sim.aspx.
[31] R. Gelabert, M. Moreno, J.M. Lluch, A. Lledós, Determination of the temperature dependence of the H–D spin–spin coupling constant and the isotope effect on the proton chemical shift for the compressed dihydride complex [Cp*Ir(P–P)H2] 2+, Chem. Phys. 241 (1999) 155–166.
[32] G.J. Kubas, Fundamentals of H2 binding and reactivity on transition metals underlying hydrogenase function and H2 production and storage, Chem. Rev. 107 (2007) 4152–4205.
[33] R.H. Morris, Estimating the wavenumber of terminal metal-hydride stretching vibrations of octahedral d6 transition metal complexes, Inorg. Chem. 57 (2018) 13809–13821.
[34] B.R. Bender, G.J. Kubas, L.H. Jones, B.I. Swanson, J. Eckert, K.B. Capps, C.D. Hoff, WHy Does D2 Bind Better Than H2? A Theoretical And Experimental Study Of The Equilibrium Isotope Effect on H2 binding in a M(η2 -H2) Complex. Normal Coordinate Analysis of W(CO)3(PCy3)2(η2 -H2), J. Am. Chem. Soc. 119 (1997) 9179–9190.
[35] G.J. Kubas, J.T. Hynes, J.P. Klinman, H.-H. Limbach, R.L. Schowen (Eds.), The Extraordinary Dynamic Behavior and Reactivity of Dihydrogen and Hydride in the Coordination Sphere of Transition Metals, Hydrogen-Transfer Reactions, Wiley-VCH Verlag GmbH & Co. KGaA: Weinheim, Germany, 2007, pp. 603–637.
[36] G.J. Kubas, MetAl Dihydrogen And σ-Bond Complexes: Structure, Theory, and Reactivity, Spring Science & Business Media, 2001.
[37] M.K. Chopra, F. Wong, G. Jia, N.-T. Yu, Detection of an unusually low ν(H-H) stretching mode in the molecular dihydrogen complex [Ru(C5H5)(Ph2PCH2PPh2)(η 2 -H2)]BF4 by near infrared fourier-transform raman spectroscopy, J. Mol. Struct. 379 (1996) 93–98.
[38] M.A. Esteruelas, M.P. Gay, V. Lezáun, M. Oliván, E. Oñate, Tuning the nature and formation of Bis(dihydrogen)–osmium species, Organomet 37 (2018) 367–379.
[39] N. Schloerer, V. Pons, D.G. Gusev, D.M. Heinekey, Structure and dynamics of a compressed dihydride complex of osmium, Organomet 25 (2006) 3481–3485.
[40] M.A. Esteruelas, C. Garc a-Yebra, J. Mart n, E. Oñate, E. mer, fac, and bidentate coordination of an Alkyl-POP ligand in the chemistry of nonclassical osmium hydrides, Inorg. Chem. 56 (2017) 676–683.
[41] C.L. Gross, D.M. Young, A.J. Schultz, G.S. Girolami, Neutron diffraction study of the ‗elongated' molecular dihydrogen complex [(C5Me5)Os(H2)H2(PPh3)]+, Dalton Trans. 18 (1997) 3081–3082.
[42] C.L. Gross, G.S. Girolami, Synthesis and NMR studies of [(C5Me5)Os(L)H2(H2) +] complexes. Evidence of the adoption of different structures by a dihydrogen complex in solution and the solid state, Organomet 26 (2007) 1658–1664.
[43] C.E. Webster, C.L. Gross, D.M. Young, G.S. Girolami, A.J. Schultz, M.B. Hall, J. Eckert, Electronic and steric effects on molecular dihydrogen activation in [CpOsH4(L)]+ (L = PPh3, AsPh3, and PCy3), J. Am. Chem. Soc. 127 (2005) 15091–15101.
[44] J. Eckert, C.M. Jensen, G. Jones, E. Clot, O. Eisenstein, An extremely low barrier to rotation of dihydrogen in the iridium complex IrClH2(η2 -H2)(PiPr3)2, J. Am. Chem. Soc. 115 (1993) 11056–11057.